water

MDPI

Review

Three-Dimensional Numerical Modelling of Real-Field Dam-Break Flows: Review and Recent Advances

Andrea Maranzoni [1,*] and Massimo Tomirotti [2]

[1] Department of Engineering and Architecture, University of Parma, 43124 Parma, Italy
[2] Department of Civil, Environmental, Architectural Engineering and Mathematics, University of Brescia, 25121 Brescia, Italy; massimo.tomirotti@unibs.it
* Correspondence: andrea.maranzoni@unipr.it

Abstract: Numerical modelling is a valuable and effective tool for predicting the dynamics of the inundation caused by the failure of a dam or dyke, thereby assisting in mapping the areas potentially subject to flooding and evaluating the associated flood hazard. This paper systematically reviews literature studies adopting three-dimensional hydrodynamic models for the simulation of large-scale dam-break flooding on irregular real-world topography. Governing equations and numerical methods are analysed, as well as recent advances in numerical techniques, modelling accuracy, and computational efficiency. The dam-break case studies used for model validation are highlighted. The advantages and limitations of the three-dimensional dam-break models are compared with those of the commonly used two-dimensional depth-averaged ones. This review mainly aims at informing researchers and modellers interested in numerical modelling of dam-break flow over real-world topography on recent advances and developments in three-dimensional hydrodynamic models so that they can better direct their future research. Practitioners can find in this review an overview of available three-dimensional codes (research, commercial, freeware, and open-source) and indications for choosing the most suitable numerical method for the application of interest.

Keywords: dam break; flooding; numerical modelling; real-world topography; review; three-dimensional models

Citation: Maranzoni, A.; Tomirotti, M. Three-Dimensional Numerical Modelling of Real-Field Dam-Break Flows: Review and Recent Advances. *Water* **2023**, *15*, 3130. https://doi.org/10.3390/w15173130

Academic Editor: Anargiros I. Delis

Received: 22 June 2023
Revised: 25 August 2023
Accepted: 27 August 2023
Published: 31 August 2023

1. Introduction

Dam-break floods are caused by the uncontrolled release of water stored in a reservoir due to a total or partial collapse of a constructed or natural dam. Such phenomena can result in potentially catastrophic consequences and many more casualties than other kinds of floods and disasters (e.g., [1,2]). Zhang et al. [3] documented 1443 failures of constructed dams and 1044 failures of landslide dams worldwide over the past two centuries and provided a list of the 20 most significant dam failures (each causing more than 500 casualties), resulting in more than 44,000 fatalities. Among these 20 selected dam disasters, the most catastrophic one is the 1975 Banqiao dam failure (China), which led to the inundation of an area of approximately 12,000 km^2 and the loss of more than 26,000 lives, followed by the disasters of the Vajont dam (Italy) in 1963, the South Fork dam (US) in 1889, and the Machhu-II dam (India) in 1979, each with more than 2000 casualties [1,3,4]. In addition, dam-break flooding can cause huge economic losses and extensive environmental damage [5]. For example, the 1976 Teton dam disaster (US) resulted in only 11 fatalities, but the flood covered an area of 77 km^2 and reached up to 250 km downstream of the dam, causing more than USD 400 million of damage [6].

Accordingly, the assessment of the flooding hazard associated with hypothetical dam-break scenarios has gained great importance and attracted considerable attention in the last decades, both in engineering practice (e.g., [7,8]) and research (e.g., [9–12]), for dam-break flood risk management, emergency response, and flood hazard mitigation planning.

In principle, a dam-break problem can be studied using either an experimental [13] or a mathematical modelling approach [14,15], or both together (e.g., [16]). However, numerical modelling has become attractive and increasingly popular due to its flexibility and cost-effectiveness and the continuous growth of computing capacities, which allows the processing of a large amount of data and solving mathematical models of great complexity and significant predictive capability [17]. Moreover, the current availability of several commercial and freeware Computational Fluid Dynamics (CFD) software codes, equipped with friendly interfaces and including effective pre- and post-processing tools, facilitates the diffusion of numerical models in flood hazard analyses [18]. The high-cost and time-consuming complex operations required to carry out accurate laboratory experimentation have determined that the physical modelling approach is currently mainly adopted to obtain experimental data useful for the validation of numerical models [13,14].

Usually, dam-break flood hazard assessment and mapping are performed using depth-averaged two-dimensional (2D) models, which solve the 2D shallow water equations (SWEs) through finite difference, finite volume, or finite element methods (e.g., [15,19–21]) to predict relevant hydraulic quantities associated with flood hazard (namely, maximum flood depth and velocity). Despite the simplifying assumptions underlying the 2D SWEs, there are many computational challenges in numerically solving these equations, such as shock-capturing capability, treatment of wet and dry fronts, treatment of bottom and friction source terms, reproduction of flow regime transitions, and preservation or achievement of stationary or steady-flow conditions. In any case, the SWEs strictly apply to flows with no significant curvature of the free surface and negligible vertical acceleration (and hence with nearly hydrostatic pressure distribution) over small bottom slopes (e.g., [21,22]). However, in gravity-driven geophysical flows, the terrain may be very steep, at least locally, especially in mountain regions or near topographic singularities [23–25]. Moreover, the hydrostatic pressure assumption is violated in curvilinear flows, which can also occur as a result of dam failures, especially during the first stages of the motion (e.g., [26,27]) or in case the flooding wave propagates in the presence of bends (e.g., [28]), contractions (e.g., [29,30]), bottom singularities (e.g., [31,32]), or obstacles and structures (e.g., [33–35]). For example, Figure 1 shows two pictures of the impact of a dam-break wave against a prismatic block [34]. Such a physical process is characterised by marked three-dimensional (3D) features.

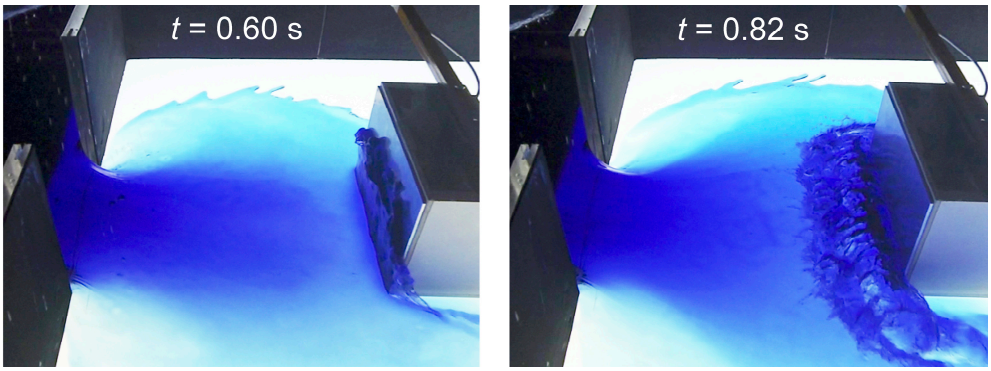

Figure 1. Three-dimensional features of a dam-break wave impacting a structure. The pictures were taken during the laboratory investigation performed by Aureli et al. [34]. Time t starts from the sudden gate removal.

Local 3D effects cannot be reproduced by the 2D SWEs [36], with consequent possible limitations in the predictive capability of 2D shallow-water models and inaccuracies in the prediction of the relevant hydraulic variables, such as flood inundation extent, maximum flood depths, and impact loads on structures [37]. More general formulations of the 2D depth-averaged SWEs have been proposed in the literature to overcome this drawback without resorting to more computationally expensive 3D models. In these enhanced formulations, some of the restrictive assumptions of the classic shallow-water model are relaxed

while retaining its robustness and simplicity. For example, steep-slope SWEs (SSSWEs) were introduced to simulate shallow flows over steep terrain (e.g., [24,25,38]). Boussinesq-type models (e.g., [23,39,40]), as well as vertically averaged and moment (VAM) equations (e.g., [41]) or depth-averaged equations incorporating an "enhanced" gravity (e.g., [42,43]), can be used to simulate non-hydrostatic flows, preserving the vertical momentum balance and including the effect of the vertical flow acceleration.

Recent advances in computing performance have fostered the application of 3D numerical models [44], which offer an improved predictive capability [45] and a more accurate description of the flow features, especially where vertical flow acceleration cannot be neglected and the pressure distribution is far from hydrostatic [19]. Three-dimensional models with different degrees of complexity (and, consequently, different computational costs) can be used, namely [40] direct numerical simulation (DNS) models, which numerically solve the Navier–Stokes equations (NSEs), resolving all turbulence spatial and temporal scales; large-eddy simulation (LES) models, which solve the filtered NSEs, thus ignoring the smallest length scales; and models that solve the Reynolds-averaged Navier–Stokes equations (RANS), coupled with a closure turbulence model [46]. DNS and LES models are significantly more computationally expensive than the RANS ones, especially at the high Reynolds numbers encountered in environmental free-surface flows. Therefore, the application of DNS and LES models in this field is feasible only in limited domains [19]. Consequently, RANS solvers are the most common choice for large-scale real-world dam-break flood simulations. However, since the flow depth does not explicitly appear in the basic equations of 3D models, great care has to be devoted to spatial discretization in the vertical direction, and additional computational effort is required for free surface tracking [37]. Several free-surface-tracking techniques have been proposed in the literature. The best known are the Volume of Fluid (VOF; [47]) and the Level Set [48] methods (or a combination of the two in coupled Level Set–VOF methods; e.g., [49]). The VOF model is the most popular in dam-break flow simulations [50]. An alternative strategy to solve the 3D governing equations, avoiding the construction of a computational mesh and the adoption of complex free-surface-tracking algorithms, is based on meshless particle-based methods, such as Smoothed Particle Hydrodynamics (SPH; [51]), which has also been applied in the modelling of dam-break flow (e.g., [52,53]), even on real-world topography, and other environmental applications [54,55].

However, the high computational cost of 3D models is still a significant limitation, especially in large-scale field studies or when high spatial accuracy is required. This limitation has hindered the diffusion of 3D models in the past for real-field applications, favouring the 2D depth-averaged ones. Hence, high-performance computing, such as parallel or Graphics Processing Unit (GPU) computing, is today a valuable support to enhance the computational efficiency of 3D models and reduce computational time.

Dam-break models (both 2D and 3D) are usually validated against experimental data of laboratory test cases [13], which, however, are typically schematic (e.g., [44,56]) or include isolated singularities (e.g., [50,57–59]). Instead, real dam-break events involve irregular topography and constitute far more challenging benchmarks for numerical models. However, well-documented historical dam-break events are scarce and often characterised by uncertain available information [14], making their use arduous for complete validation of the numerical models (especially for 3D ones, in which several parameters are involved). Nonetheless, they provide valuable information about the different degrees of reliability of the models in reproducing dam-break flow features over real-world topography.

Table 1 provides a comparative summary of the advantages and shortcomings of 3D and depth-averaged 2D models. Given the increasing diffusion of 3D CFD models and their improved predictive capabilities compared with the 2D ones, this review focuses on 3D modelling of large-scale real-field dam-break floods.

Table 1. Summary and comparison of the advantages and shortcomings of 3D and 2D models.

Model	Advantages	Shortcomings
2D depth-averaged	Easy to build and implement Computationally cheap Few parameters to calibrate (roughness) Robust and stable	Limitations due to the shallow-water assumptions (hydrostatic distribution of pressure and small bottom slopes)
3D	High accuracy (mild restrictive assumptions) Reproduction of non-hydrostatic effects	Laborious to build and implement Complex calculations Computationally expensive Several parameters involved

Figure 2 shows a sketch of the methodological framework of this study. The systematic review is restricted to publications focusing on 3D CFD modelling of dam-break flow and providing application examples of numerical simulation of dam-break flooding over irregular real-world topography. A comparative analysis is performed on the documents collected, and the information relevant to 3D CFD modelling is reported in tabular form (Section 2). The results of the analysis allow statistical information on key items of the reviewed documents (such as year of publication, software status, model type, and numerical scheme) to be obtained. The discussion of the review findings is centred on the following aspects: improvements in simulation accuracy, model validation and calibration, improvements in computational efficiency, and improvements in result visualization (Section 3). Finally, conclusions are drawn, outlining implications that can facilitate practical applications and future research on 3D CFD models for the simulation of large-scale dam-break flooding on irregular real-world topography (Section 4).

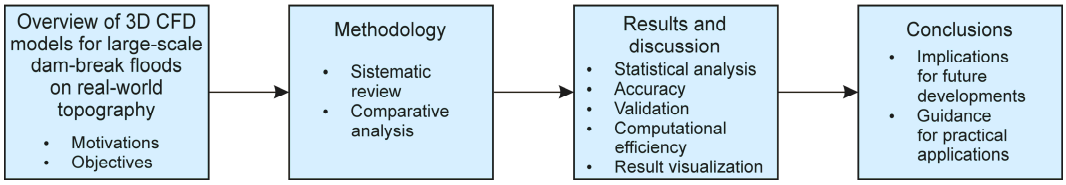

Figure 2. Schematic of the methodological framework of this review study.

1.1. Motivations of the Present Review

There is a vast literature overviewing, describing, comparing, and evaluating flood inundation numerical models for flood risk assessment and water resources management (e.g., [15,18,19]). For instance, Teng et al. [15] conducted a comprehensive review of different modelling approaches (empirical, hydrodynamic, and simplified conceptual models), highlighting their advantages and drawbacks and discussing the sources of uncertainty in flood inundation modelling. Mudashiru et al. [18] provided a similar overview, focusing on flood hazard mapping. Bates [19] surveyed recent advances in floodplain inundation modelling, discussing the ability of the numerical models to reproduce the physical aspects of the flooding process. Luo et al. [60] and Mignot and Dewals [61] limited the area of focus, reviewing specifically urban flood simulation models and analysing their hydrologic and hydrodynamic component modules. More recently, Kumar et al. [62] and Avila-Aceves et al. [63] offered a broad overview of different modelling approaches and numerical techniques for simulating large-scale inundations, providing insight into their strengths and weaknesses.

Only a few of the previously mentioned reviews touch on the use of 3D hydrodynamic models for flood inundation simulations [15,19]. However, to our knowledge, no literature reviews exist on the specific topic of 3D hydrodynamic modelling of large-scale dam-break flows on real-world topography. Recent advances in 3D dam-break modelling, the growing

attention given to 3D CFD models in recent times due to enhanced computational efficiency, and the prospect of using 3D models extensively in engineering practice in the near future for dam-break flood risk assessment are the main motivations for this review.

1.2. Objectives of the Present Review

This review aims to inform researchers new to the field and more experienced researchers of the recent advances in 3D CFD dam-break modelling on real-world topography, thereby enabling them to have a general, updated overview of this topic. The comparative analysis of the relevant references selected can help modellers, practitioners, emergency response agencies, and dam owners remain up to date on the latest developments in dam-break simulation tools and choose the most suitable numerical model for the specific application of interest. Finally, this review study provides state-of-the-art information to direct future research on 3D dam-break numerical modelling for real field applications.

2. Review and Comparative Analysis

A systematic and careful search was performed in the most well-known scientific databases (based on the keywords: "dam-break", "3D numerical modelling", "real topography", "complex topography", and similar) to ensure wide coverage of the existing literature on 3D numerical modelling of large-scale dam-break flows over real-world topography. Mainly the academic literature (i.e., journal or conference articles) was considered; the grey literature was not included.

The documents retrieved in the literature survey are arranged in Table 2, including studies on dam spillway flows or overtopping flows reporting the numerical simulation of the subsequent flood propagation downstream. Table entries are organised in chronological order. References that contain multiple real-world case studies are repeated for each of these and appear in different rows of the table (i.e., one row for each case study).

Table 2 provides the following, most significant information.

(1) *Relevant references retrieved*. Multiple references are reported in the same table row when details providing a complete description of the case study analysed can be obtained from various articles. In the case of duplicate studies, the most complete one was considered, and subordinately, the earliest one.

(2) *Code/software name*, if available. Besides well-known commercial (e.g., TELEMAC-3D [64]; FLOW-3D [65]) or open-source CFD software codes (e.g., OpenFOAM [66]; DualSPHysics [67]) widely used in many hydrodynamic applications, numerical codes (sometimes with no name) developed by universities or research centres for research purposes (e.g., [68]) appear in the table.

(3) *Basic equations of the simulation models*: in order of increasing complexity, the Euler equations, the Navier–Stokes equations, and the RANS equations for incompressible flow. In the last case, a closure turbulence model is coupled with the governing equations. Lattice Boltzmann methods (based on the Boltzmann equation and simulating the flow through collision models of fictitious particles moving on a discrete lattice grid) are used more rarely in dam-break flooding simulations. The table also reports the rheological model coupled with the hydrodynamic equations in mudflow modelling of tailings dam breaks and the erosional model used in the analysis of geomorphic dam-break flows over an erodible bottom.

(4) *Numerical methods* used for spatial and temporal discretization of the model equations. The indication of the numerical scheme used for the simulations is accompanied by the specification of the discretization technique (finite volume, finite element, SPH, etc.).

(5) *Dam-break case studies* considered to demonstrate the applicability of the numerical models. Some case studies concern historical dam-break events, while others concern hypothetical dam failures. The former case studies, if well documented, can be used for model validation and to evaluate the model's ability to reproduce real-field dam-break flooding. Case studies of the latter type concern model applications to real-world situations, mainly aimed at assessing dam-break flood hazards in potentially floodable areas.

(6) *Details about the computational domain and the spatial resolution* adopted in the numerical simulation of the case studies considered (i.e., the number of grid cells in mesh-based models or fluid particles in meshless models). The mesh type (structured or unstructured) and the shape of the grid elements are specified for mesh-based models.

(7) *Outcomes of the numerical modelling*. Typically, model results include flooded areas, flood depth contour maps and flow velocity fields at selected times, contour maps of the maximum values of flood depth and velocity magnitude, time series of flood depth and flow velocity at given locations, and time series of flow discharge at selected cross-sections.

(8) *Focus of the studies*. The focus may be on the model validation, the prediction or reconstruction of the inundation dynamics, or the 3D effects due to flow curvature. Different aspects are sometimes examined contextually.

(9) *Computational efficiency*. The simulation (physical) time and the corresponding computational run-time are reported for the case studies (when these data are available), along with strategies implemented to improve computational efficiency.

(10) *Publication year*. This bibliographic information is useful to place each contribution in time, outlining the evolution of the numerical models over time and research trends. If multiple references are associated with a single table row, the publication year of the oldest one is reported.

(11) *Status of the CFD model*. This can be commercial, freeware, open-source, or research.

Table 2. Overview of studies on 3D hydrodynamic modelling of large-scale dam-break flooding over real-world topography.

(1) Reference	(2) Model Name	(3) Model Type [1]	(4) Numerical Method [2]	(5) Case Study	(6) Computational Domain and Elements	(7) Output Data	(8) Focus of the Study	(9) Computational Efficiency [3]	(10) Year	(11) Status
Roubtsova and Kahawita [69] *	N/A	Navier–Stokes and continuity equations	Weakly compressible SPH	Historical 1963 overtopping of the Vajont dam (Italy) Volume of the rockslide: 270 million m^3 Stored water volume: 115 million m^3 (reservoir water level provided) Overtopping water volume: 30 million m^3	Modelled area extent: N/A (the reservoir and the Vajont River downstream) Number of particles: N/A Particle spacing: N/A	Water surface at selected times; transverse water surface profiles at a selected cross-section in the reservoir	Performance of the numerical technique Reconstruction of the event Comparison with field observations	Simulation time: 220 s Run time/ simulation time: ~74	2006	Research
Cleary et al. [70]; Prakash et al. [71]	N/A	Navier–Stokes and continuity equations	Weakly compressible SPH	Historical 1928 St. Francis dam break (California) Water volume: 47 million m^3	Modelled area extent: the reservoir and a valley stretch downstream of the dam Number of particles: 1.4×10^6 Particle spacing: 4 m	Flow fields (velocity magnitude) and flooded areas at selected times; motion of wall fragments; flow discharge hydrograph at the dam site; flood arrival times and maximum flood depths at selected locations	Flooding dynamics for different collapse scenarios Comparison with field data Modelling of the motion of dam wall blocks 3D effects Sensitivity on particle resolution (4 m; 6 m; 8 m)	Simulation time: 25 min Run time/ simulation time: N/A	2010	Research
Cleary et al. [70]; Ye et al. [72]; Cleary et al. [73]	N/A	Navier–Stokes and continuity equations	Weakly compressible SPH	Hypothetical Geheyan dam break (China) Water volume: 3.12 billion m^3 Different dam failure scenarios	Modelled area extent: the reservoir and a valley stretch downstream of the dam Number of particles: 1.3×10^6 (fluid), 1.9×10^6 (boundaries) Particle spacing: 15 m (fluid), 30 m (boundaries)	Flow fields (velocity magnitude) and flooded areas at selected times (different views); discharge hydrograph at the dam site; flow discharge hydrographs at selected sections; flood depth hydrographs at selected locations	Flooding dynamics 3D effects Effect of different dam failure scenarios Modelling of the motion of dam wall blocks	Simulation time: 60 min Run time/ simulation time: N/A	2010	Research
Lee et al. [74] *	N/A	Navier–Stokes and continuity equations	Weakly compressible and truly incompressible SPH	Ski-jump spillway of the Goulours dam (France)	Modelled area extent: The reservoir (assumed to be of prismatic shape) and ~250 m-long valley reach downstream of the dam (according to a 1:20 scale physical model) Number of particles: 9.366×10^5 (wall particles: 2.169×10^5; fictitious particles: 2.196×10^5) Particle spacing (initial): 0.2 m	Spillway flow dynamics; flooded areas at selected times	Qualitative reconstruction of the spillway process Spillway flow features	Simulation time: 16 s Run time/ simulation time: ~2.7×10^4	2010	Research

Table 2. *Cont.*

(1) Reference	(2) Model Name	(3) Model Type [1]	(4) Numerical Method [2]	(5) Case Study	(6) Computational Domain and Elements	(7) Output Data	(8) Focus of the Study	(9) Computational Efficiency [3]	(10) Year	(11) Status
Caboussat et al. [75]	N/A	Incompressible Navier–Stokes equations coupled with VOF	Finite element; implicit time splitting scheme (advection and diffusion steps)	Historical 1959 Malpasset dam break (France) Water volume: 50 million m^3	Modelled area extent: 17.5 km × 9 km Unstructured grid of tetrahedral cells (diffusion step) Number of cells: 1.716×10^6 Spatial resolution: 5 m Structured grid of cubic cells (advection step) Number of cells: N/A Spatial resolution: 2 m	Flooded areas and flow velocity fields at selected times; maximum flood depths and arrival times at selected points	Comparison with physical model data	Simulation time: >8 min Run time/ simulation time: 600	2011	Research
Caboussat et al. [75]	N/A	Incompressible Navier–Stokes equations coupled with VOF	Finite element; implicit time splitting scheme (advection and diffusion steps)	Hypothetical Grande-Dixence dam break (Switzerland) Water volume: 400 million m^3	Modelled area extent: 28.9 km × 5.75 km Unstructured grid of tetrahedral cells (diffusion step) Number of cells: 13.876×10^6 Spatial resolution: 50 m Structured grid of cubic cells (advection step) Number of cells: N/A Spatial resolution: 10 m	Flooded areas and flow velocity fields at selected times; flood depth contour maps at selected times	Inundation dynamics	Simulation time: 10 min Run time/ simulation time: N/A	2011	Research
Vassilevski et al. [76]	N/A	Incompressible Navier–Stokes equations coupled with grid level set function (for free surface tracking); Herschel–Bulkley rheological relation for viscoplastic fluids	Finite difference/ finite volume; Chorin–Temam-Yanenko time splitting scheme	Hypothetical Sayano–Shushenskaya partial dam-break (Russia) Water volume: N/A	Modelled area extent: the reservoir and a valley stretch downstream of the dam Structured octree staggered grid	Flood depth hydrographs at selected points; time series of the bottom pressure at the base of the spillway	Dam-break flow	Simulation time: 100 s Run time/ simulation time: N/A	2012	Research
Vacondio et al. [77] *	DualSPHysics	Navier–Stokes and continuity equations	Weakly compressible SPH	Historical 1963 overtopping of the Vajont dam (Italy) Volume of the rockslide: 310 million m^3 Stored water volume: N/A (reservoir water level provided)	Modelled area extent: the reservoir and a valley stretch downstream of the dam Number of particles: 3.954×10^6 (bottom particles: 2.144×10^6; rockslide particles: 1.274×10^5; fluid particles: 1.683×10^6) Particle size: 5 m	Water surface elevation at selected times; maximum run-up on the reservoir side; water surface elevation in the residual lake; flow velocity field; overflow hydrograph	Reconstruction of the wave generated by the Vajont rockslide and of the dam-overtopping phenomenon Comparison with field observations	Simulation time: 21 min Run time/ simulation time: 177 Parallelization on GPU	2013	Open-source

Table 2. *Cont.*

(1) Reference	(2) Model Name	(3) Model Type [1]	(4) Numerical Method [2]	(5) Case Study	(6) Computational Domain and Elements	(7) Output Data	(8) Focus of the Study	(9) Computational Efficiency [3]	(10) Year	(11) Status
Zhainakov and Kurbanaliev [78]; Jainakov et al. [79]	OpenFOAM	RANS coupled with VOF; standard *k*-*ε* turbulence model	Finite volume; PIMPLE algorithm; explicit Euler first-order time discretization method	Hypothetical Andijan dam break (Uzbekistan) Water volume: N/A	Modelled area extent: 6 km × 4 km Structured mesh of hexahedral cells Number of cells: 120 × 120 × 80	Contour maps of the water volume fraction at selected times	Flood wave propagation	Simulation time: 240 s Run time/ simulation time: 135	2013	Open-source
Zhainakov and Kurbanaliev [78]; Jainakov et al. [79]	OpenFOAM	RANS coupled with VOF; standard *k*-*ε* turbulence model	Finite volume; PIMPLE algorithm; explicit Euler first-order time discretization method	Hypothetical Papan dam break (Kyrgyzstan) Water volume: N/A	Modelled area extent: 5 km × 5 km Structured mesh of hexahedral cells Number of cells: 50 × 60 × 30	Contour maps of the water volume fraction at selected times	Flood wave propagation	Simulation time: 260 s Run time/ simulation time: 69	2013	Open-source
Džebo et al. [80]	Tis Isat	Navier–Stokes and continuity equations	Weakly compressible SPH	Hypothetical break of the embankment of the reservoir of the Kolarjev vrh pumped-storage hydropower plant (Slovenia) Water volume: 3.1 million m^3	Modelled area extent: the reservoir and a 4.5 km long valley stretch downstream Number of particles: (a) 21.890 × 10^3; (b) 174.884 × 10^3 Particle size: (a) 5 m; (b) 2.5 m	Water surface elevation at selected times; transverse water surface profiles at given cross-sections; flow depth hydrographs at selected gauge points	Flooding dynamics Comparison with 2D depth-averaged model predictions and physical model experimental data Effects of different bottom roughness values and spatial resolutions	Simulation time: 200 s Run time/ simulation time: (a) 30; (b) 981	2014	Research
Marsooli and Wu [50]	N/A	RANS coupled with VOF; Smagorinsky eddy viscosity turbulence model	Finite volume; PISO algorithm; CICSAM scheme	Flash flood in the Toce River 1:100 physical model (Italy) Controlled impulsive inflow	Modelled area extent: 5 km long reach of the Toce River (5.5 km × 1.2 km) Unstructured mesh of hexahedral cells Number of cells: 3.1 × 10^6	Flow-depth hydrographs at selected points	Comparison with experimental physical model data Comparison with 2D depth-averaged model predictions	Simulation time: 3 min Run time/ simulation time: 4100	2014	Research
Zhou et al. [81]	N/A	RANS coupled with VOF; *k*-*ε* turbulence model	Finite volume; PISO algorithm	Flash flood in the Toce River 1:100 physical model (Italy) Controlled impulsive inflow	Modelled area extent: 5 km long reach of the Toce River (50 m × 11 m in the physical model; presence of an idealised urban district) Structured mesh of prismatic cells Number of cells: 8.904 × 10^3 Spatial resolution: 1 m (horizontal) 10^{-2} m (vertical)	Water depth hydrographs at selected gauge points	Validation (comparison with physical model experimental data)	Simulation time: 60 s Run time/ simulation time: N/A	2014	Research

Table 2. *Cont.*

(1) Reference	(2) Model Name	(3) Model Type [1]	(4) Numerical Method [2]	(5) Case Study	(6) Computational Domain and Elements	(7) Output Data	(8) Focus of the Study	(9) Computational Efficiency [3]	(10) Year	(11) Status
Zhou et al. [81]	N/A	RANS coupled with VOF; k-ε turbulence model	Finite volume; PISO algorithm	Hypothetical Dongwushi dam break (China) Water volume: 161.5 million m^3 (Hypothetical dam break of four other dams in the same Haihe River basin, China)	Modelled area extent: upper reach of the valley of the Fuyang River Unstructured mesh of hexahedral cells Number of cells: 79.513×10^3	VOF spatial distribution at selected times; flow velocity field at selected times; flow discharge hydrographs at selected cross-sections (including the dam site); flood depth spatial distribution at selected times	Flood wave propagation Dam-break risk analysis	Simulation time: ~47 h Run time/ simulation time: N/A	2014	Research
Biscarini et al. [82]	OpenFOAM	RANS coupled with VOF; k-ε turbulence model	Finite volume; PISO algorithm; MULES scheme	Historical 1959 Malpasset dam break (France) Water volume: 50 million m^3	Modelled area extent: 17.5 km × 10 km Unstructured mesh Number of cells: 2.203×10^6 Spatial resolution: N/A	Arrival time at selected points; flood hydrographs at selected points; flooded area at selected times; transverse free surface profiles at a river bend cross-sections; velocity fields in selected areas	Comparison with experimental (field and physical model) data 3D effects at sharply curved river bends	Simulation time: 40 min Run time/ simulation time: N/A	2016	Open-source
TELEMAC Modelling System [83]	TELEMAC-3D	Navier–Stokes and continuity equations (Boussinesq approximation)	Finite element; three-fractional-step algorithm	Historical 1959 Malpasset dam break (France) Water volume: 50 million m^3	Modelled area extent: 17 km × 9 km Unstructured horizontal mesh of triangular elements Number of cells: (a) 26×10^3; (b) 104×10^3 Vertical mesh: 2 or 6 layers regularly spaced in the vertical direction	Flood depth contour maps at selected times; flood depth hydrographs at selected locations	Flood wave propagation	Simulation time: 4000 s Run time/ simulation time: N/A	2016	Freeware
Amicarelli et al. [84]	SPHERA	Continuity equations of the fluid and solid incompressible phases + volume balance equation; momentum equations of the fluid and solid phases; momentum equation for the mixture	Weakly-compressible SPH; Leapfrog time integration scheme	Erosional dam-break demonstrative ICOLD benchmark Water volume: N/A (reservoir water level provided)	Modelled area extent: 24.627 km × 9.855 km Mobile bottom downstream of the dam (granular material of fixed characteristics) Number of particles: 6.8×10^5 Particle spacing: 4 m	3D distribution of the particles and velocity fields at selected times; maps of maximum values of mixture depth and specific flow rate; water and bed-load flow rate and mixture depth hydrographs at selected cross-sections	Dynamics of the phenomenon	Simulation time: 25 min Run time/ simulation time: N/A	2017	Open-source

Table 2. *Cont.*

(1) Reference	(2) Model Name	(3) Model Type [1]	(4) Numerical Method [2]	(5) Case Study	(6) Computational Domain and Elements	(7) Output Data	(8) Focus of the Study	(9) Computational Efficiency [3]	(10) Year	(11) Status
Wang et al. [85]	N/A	RANS coupled with VOF; k-ε turbulence model	Finite volume; PISO algorithm	Flash flood in the Toce River 1:100 physical model (Italy) Controlled impulsive inflow	Modelled area extent: 5 km long reach of the Toce River (50 m × 11 m in the physical model; two idealised urban district configurations) Unstructured mesh of polyhedral cells Number of cells: ~2×10^5 Spatial resolution: 0.1 m	Computational time; computational error; water depth hydrographs at selected gauge points	Validation (comparison with physical model experimental data) Dam-break flooding of an urban area Comparison of computational performance of different mesh types (polyhedral, tetrahedral, hexahedral)	Simulation time: 60 s Run time/ simulation time: ~20	2017	Research
Wang et al. [85]	N/A	RANS coupled with VOF; k-ε turbulence model	Finite volume; PISO algorithm	Hypothetical dam break of an urban reservoir (SZ City, China) Water volume: 94 million m^3	Modelled area extent: 40.12 km^2 area Unstructured mesh of polyhedral cells Number of cells: 4.229×10^6	VOF spatial distribution at selected times; flood depth and flow velocity hydrographs at selected sites in the urban area; velocity and vorticity fields; maximum flood depth and flow velocity contour maps	Dam-break flooding of an urban area	Simulation time: 5 h Run time/ simulation time: N/A	2017	Research
Wang et al. [86]	DualSPHysics	Navier–Stokes and continuity equations	Weakly compressible SPH	Historical 2015 Fundão tailings dam break (Brazil) Released tailings volume: 32 million m^3	Modelled area extent: N/A (the pond and the area around) Number of particles: 2.988×10^6 (fluid) 18.132×10^6 (boundaries) Particle spacing: 3 m	Flow fields (velocity magnitude) and flooded areas at selected times; flow depth, velocity, and impact pressure time series at a selected location	Tailings flow dynamics Comparison with field data	Simulation time: 30 min Run time/ simulation time: N/A Parallelization on GPU	2018	Open-source
Wang et al. [86]	DualSPHysics	Navier–Stokes and continuity equations	Weakly compressible SPH	Hypothetical dam break of an operating overhead tailings pond (China) Pond capacity: 33 million m^3	Modelled area extent: N/A (the pond and the area around) Number of particles: 4.463×10^6 (fluid) 3.9×10^6 (boundaries) Particle spacing: 3 m	Flow fields (velocity magnitude) and flooded areas at selected times; flow depth, velocity, and impact pressure time series at a selected location	Tailings flow dynamics	Simulation time: 10 min Run time/ simulation time: N/A Parallelization on GPU	2018	Open-source

Table 2. *Cont.*

(1) Reference	(2) Model Name	(3) Model Type [1]	(4) Numerical Method [2]	(5) Case Study	(6) Computational Domain and Elements	(7) Output Data	(8) Focus of the Study	(9) Computational Efficiency [3]	(10) Year	(11) Status
Zhang et al. [87]	N/A	Navier–Stokes and continuity equations (Boussinesq approximation)	Finite element; θ time-stepping method	Hypothetical dike-break flooding on a realistic topography (fixed inflow velocity)	Modelled area extent: 100 m × 100 m Unstructured horizontal mesh of triangular elements; spatial resolution: 5 m Vertical mesh: 1 layer Unstructured mesh of tetrahedral cells Number of cells: 3.114×10^3	Velocity fields and flooded areas at selected times	Flood wave propagation 3D effects	Simulation time: 7 min Run time/ simulation time: N/A	2018	Research
Zhang et al. [87]	N/A	Navier–Stokes and continuity equations (Boussinesq approximation)	Finite element; θ time-stepping method	Hypothetical dike-break flooding in a realistic urban area (flow velocity through the breach: 0.1 m/s)	Modelled area extent: 5.495 km × 2.5 km Unstructured horizontal mesh of triangular elements; spatial resolutions: (a) 30–50 m; (b) 60–100 m; (c) 120–200 m Vertical mesh: 1 layer Unstructured mesh of tetrahedral cells Number of cells: (a) 9376; (b) 3024; (c) 816	Flooded areas, flood depth contour maps, and velocity fields at selected times; flood depth hydrographs at selected points	3D effects Sensitivity to the mesh resolution	Simulation time: 6 h Run time/ simulation time: (a) 17.5; (b) 3.5; (c) 0.3	2018	Research
Chen et al. [88]	LS-DYNA	Navier–Stokes and continuity equations; material with fluid-elastoplastic properties	SPH	Historical 1985 Stava tailings dam break (Italy) Released tailings volume: 185×10^3 m^3	Modelled area extent: the pond and a 4.2 km long stretch of the valley Number of particles: 11.119×10^3 (fluid) Particle spacing: 2.5 m	Flow fields (velocity magnitude) and flooded areas at selected times; average velocity profile of the debris flow front; velocity field near the check dam; arrival time at an observation point; final deposition zones; impact force hydrographs (considering a single or multiple check dams)	Debris flow dynamics Fluid–structure interactions Comparison with other numerical results Effect of the presence of hypothetical check dams (rigid indestructible dams or concrete destructible dams) placed at different positions	Simulation time: N/A Run time/ simulation time: N/A	2019	Commercial
Kurbanaliev et al. [89]	OpenFOAM	RANS coupled with VOF; standard k-ε turbulence model	Finite volume; PISO algorithm; explicit Euler first-order time discretization method	Hypothetical dam-break flow in the Willow Creek Mountain area (California) Water volume: N/A	Modelled area extent: ~8 km × 3 km Mesh of hexahedral cells Number of cells: 0.45×10^6	Maps of the water volume fraction at selected times; flood depth hydrographs at selected points	Flood wave propagation	Simulation time: 400 s Run time/ simulation time: ~45	2019	Open-source

Table 2. *Cont.*

(1) Reference	(2) Model Name	(3) Model Type [1]	(4) Numerical Method [2]	(5) Case Study	(6) Computational Domain and Elements	(7) Output Data	(8) Focus of the Study	(9) Computational Efficiency [3]	(10) Year	(11) Status
Issakhov and Zhandaulet [90]	N/A	RANS coupled with VOF; three incompressible phases for the simulation of mixed water–mud flow: two Newtonian fluids (air and water) and a non-Newtonian liquid; realizable k-ω turbulence model	Finite volume; PISO algorithm	Hypothetical Mynzhylky erosional dam break (Kazakhstan) Water volume: 50×10^3 m^3	Modelled area extent: 17×10^3 m^2, 1.317 km long river reach downstream of the dam Homogeneous mud layer of fixed thickness downstream of the dam Structured mesh of tetrahedral cells Number of cells: 2.433×10^6 Spatial resolution: 0.5 m	Flood depth hydrographs at selected points; water surfaces and inundated areas at selected times (for different mud layer thicknesses)	Flood wave (with mud) propagation Effect of the initial mud layer thickness	Simulation time: 60 s Run time/ simulation time: N/A	2020	N/A
Munoz and Constantinescu [37]	STAR-CCM+	RANS coupled with VOF; realizable k-ε turbulence model	Finite volume; SIMPLE algorithm	Hypothetical Coralville dam-break (USA) Water volume: N/A (reservoir water level provided)	Modelled area extent: 18 km long river reach downstream of the dam and floodplains Lake: unstructured grid with polyhedral cells; spatial resolution: 100 m River and floodplains: unstructured grid with prismatic cells; multi-resolution Number of cells: 18×10^6	Flooded areas at different times; free surface profile along the river at peak flood extent; discharge hydrographs at selected river sections; unit discharge transverse profiles in selected cross-sections at peak flood extent; details of the velocity field	Flood wave propagation 3D effects Comparison with 2D depth-averaged model predictions Recalibration of the 2D model parameter to improve the agreement between 2D and 3D model results	Simulation time: 5 h Run time/ simulation time: 144 Parallelization using MPI	2020	Commercial
Munoz and Constantinescu [37]	STAR-CCM+	RANS coupled with VOF; realizable k-ε turbulence model	Finite volume; SIMPLE algorithm	Hypothetical Saylorville dam break (USA) Water volume: N/A (reservoir water level provided)	Modelled area extent: 18 km long river reach downstream of the dam and floodplains Lake: unstructured grid with polyhedral cells; spatial resolution: N/A River and floodplains: unstructured grid with prismatic cells; multi-resolution Number of cells: 40×10^6	Flooded areas at different times; free surface profile along the river at the end of the simulation; discharge hydrographs at selected river sections	Flood wave propagation 3D effects Comparison with 2D depth-averaged model predictions	Simulation time: 3.75 h Run time/ simulation time: 230 Parallelization using MPI	2020	Commercial
Wang et al. [91]	DualSPHysics	Navier–Stokes and continuity equations; generalised Herschel–Bulkley–Papanastasiou rheological model	Weakly compressible SPH	Hypothetical Yujiaquan tailings dam break (China) Pond capacity: 52.55 million m^3	Modelled area extent: the pond and the area around (~2 km × 2 km) Number of particles: 3.495×10^6 (fluid) 0.936×10^6 (boundaries) Particle spacing: 2 m	Flow fields (velocity magnitude) and flooded areas at selected times	Tailings flow dynamics	Simulation time: 10 min Run time/ simulation time: N/A Parallelization on GPU	2020	Open-source

Table 2. *Cont.*

(1) Reference	(2) Model Name	(3) Model Type [1]	(4) Numerical Method [2]	(5) Case Study	(6) Computational Domain and Elements	(7) Output Data	(8) Focus of the Study	(9) Computational Efficiency [3]	(10) Year	(11) Status
Yu et al. [92]	OpenFOAM	RANS coupled with VOF; standard *k*-ε turbulence model; Bingham–Papanastasiou rheological model	Finite volume; PISO algorithm	Historical 2019 Feijão (Brumadinho) tailings dam break (Brazil) Pond capacity: 12.7 million m^3 Released tailings volume: 11.7 million m^3	Modelled area extent: N/A (suitable area around the reservoir) Unstructured mesh of hexahedral cells Number of cells: 3.242×10^6 Spatial resolution: 10 m (horizontal) 3 m (vertical)	Flow velocity magnitude contour maps at selected times; wave front motion; free surface average velocity hydrograph; flooded area	Tailings flow dynamics Comparison with field data	Simulation time: 2500 s Run time/ simulation time: N/A Parallelization using MPI (analysis of the speed-up of different numbers of processors)	2020	Open-source
Yu et al. [92]	OpenFOAM	RANS coupled with VOF; standard *k*-ε turbulence model; Bingham–Papanastasiou rheological model	Finite volume; PISO algorithm	Hypothetical A'xi gold tailings dam break (China) Pond capacity: 3.6 million m^3	Modelled area extent: N/A (suitable area around the reservoir) Unstructured mesh of hexahedral cells; number of cells: 6.657×10^6 Spatial resolution: 3 m	Flow velocity magnitude contour maps at selected times; wave front motion; free surface average velocity hydrograph; flooded area	Tailings flow dynamics	Simulation time: 800 s Run time/ simulation time: N/A Parallelization using MPI (analysis of the speed-up of different numbers of processors)	2020	Open-source
Zhuang et al. [93]	FLOW-3D	RANS coupled with VOF; RNG *k*-ε turbulence model	Finite volume	Historical landslide dam break consequent to the 2000 Yigong landslide (China) Water volume: N/A (water depth of 60 m at the barrier lake)	Modelled area extent: ~33 km long stretch of the Yigong River valley Mesh details: N/A	Flood depth contour maps at selected times; flow depth and velocity hydrographs at selected points; flow discharge at selected sections	Landslide and following landslide dam-break coupled 3D simulations Comparison with field data Flood wave propagation	Simulation time: 3 h 20 min Run time/ simulation time: N/A	2020	Commercial
Amicarelli et al. [94]	SPHERA	Euler and continuity equations	Weakly-compressible SPH	Hypothetical Alpe Gera dam break (Italy) Water volume: 68.1 million m^3	Modelled area extent: 7.9 km × 9.9 km Number of particles: N/A Particle spacing: N/A	Flooded areas; velocity fields at selected times; maximum flood depth contour map; discharge and flood depth hydrographs at selected sections	Urban flood features Comparison with experimental laboratory data Adoption of a flooding damage model	Simulation time: 50 min Run time/ simulation time: N/A	2021	Free and open-source
Karam et al. [95]	FLOW-3D	RANS coupled with VOF; RNG *k*-ε turbulence model	Finite volume	Hypothetical Attabad Lake landslide dam break (Pakistan) Water volume: 305 million m^3	Modelled area extent: N/A (stretch of the downstream valley) Multiple mesh blocks of hexahedral cells Number of cells: N/A	Flow depth hydrographs at selected sites; flow discharge hydrographs at selected cross-sections; flood inundation maps and velocity fields at selected times; flood arrival times at selected locations	Flood wave propagation	Simulation time: ~1 h 19 min Run time/ simulation time: N/A	2021	Commercial

Table 2. *Cont.*

(1) Reference	(2) Model Name	(3) Model Type [1]	(4) Numerical Method [2]	(5) Case Study	(6) Computational Domain and Elements	(7) Output Data	(8) Focus of the Study	(9) Computational Efficiency [3]	(10) Year	(11) Status
Miliani et al. [96]	N/A	Lattice Boltzmann equation with the Bhatnagar–Gross–Krook (BGK) collisional operator; interface tracking method	Lattice Boltzmann algorithm	Flash flood in the Toce River 1:100 physical model (Italy) Controlled impulsive inflow Two case studies considered: the presence of actual buildings and an idealised array of buildings	Modelled area extent: 5 km long reach of the Toce River (5.5 km × 1.2 km)	Video animations of the numerical results; flood depth hydrographs at selected gauge points	Flood wave propagation	Simulation time: N/A Run time/ simulation time: N/A	2021	Research
Ai et al. [97]	N/A	RANS coupled with a free-surface equation; non-hydrostatic and hydrostatic versions; standard k-ε turbulence model	Coupled finite volume–finite difference; explicit projection method	Flash flood in the Toce River 1:100 physical model (Italy) Controlled impulsive inflow (high-inflow and low-inflow hydrographs) Array of aligned buildings simulating a simplified urban district	Modelled area extent: 5 km long reach of the Toce River (5.5 km × 1.2 km) Unstructured mesh of prismatic cells with triangular basis in a vertical boundary-fitted coordinate system Number of cells: 1.041×10^5 (2.082×10^4 triangular elements on the bottom and 5 layers along the vertical)	Flow depth hydrographs at selected points	Non-hydrostatic effects Comparison with experimental physical model data Comparison with hydrostatic 3D model predictions	Simulation time: 1 min Run time/ simulation time: 29.4 (high-inflow hydrograph) Run time/ simulation time: 24 (low-inflow hydrograph)	2022	Research
Issakhov et al. [98]	ANSYS Fluent	RANS coupled with VOF; three incompressible phases for the simulation of mixed water–mud flow: two Newtonian fluids (air and water) and a non-Newtonian liquid; realizable k-ω turbulence model	Finite volume; PISO algorithm	Hypothetical erosional dam-break flow along the Kargalinka River (Kazakhstan) Water volume: 333.5×10^3 m^3	Modelled area extent: N/A (a stretch of the river) Homogeneous mud layer of fixed thickness downstream of the dam Structured mesh of uniform cells Number of cells: 0.985×10^6	Water surfaces and inundated areas at different times; flood depth hydrographs at selected points (for different mud layer thicknesses)	Flood wave (with mud) propagation Effect of the initial mud layer thickness	Simulation time: 34.5 s Run time/ simulation time: N/A	2022	Commercial
Yang et al. [99]	ANSYS CFX	RANS coupled with VOF; standard k-ε turbulence model; Bingham rheological model	Finite volume; PISO algorithm	Hypothetical Dagangding tailings dam break (China) Pond capacity: 3.59 million m^3 (Theoretical inflow discharge at the dam site)	Modelled area extent: N/A (selected area downstream of the dam) Unstructured mesh with tetrahedral and pentahedral cells Number of cells: 0.543×10^6	Flow fields (velocity magnitude) and flooded areas at selected times; wave front advancement and celerity in time; final deposition area and depth distribution; longitudinal and transverse profiles of the final deposit	Tailings flow dynamics	Simulation time: 2000 s Run time/ simulation time: N/A	2022	Commercial

Table 2. *Cont.*

(1) Reference	(2) Model Name	(3) Model Type [1]	(4) Numerical Method [2]	(5) Case Study	(6) Computational Domain and Elements	(7) Output Data	(8) Focus of the Study	(9) Computational Efficiency [3]	(10) Year	(11) Status
Zhuang et al. [100]	DAN3D	Hydrodynamic equations; rheological models (Bingham model)	SPH	Historical 2017 Tonglüshan tailings dam break (China) Pond capacity: 15.78 million m^3; moved slurry volume: 0.5 million m^3	Modelled area extent: ~2 km × 1.5 km area around the tailings pond Number of particles: 4×10^3 Particle spacing: N/A	Flow depth maps at different times; final deposition area and slurry depth distribution; maximum velocity magnitude map	Propagation of the tailings slurry Comparison with field data concerning the final deposition distribution of the tailings slurry Sensitivity analysis on the solid concentration of the tailings slurry	Simulation time: 300 s Run time/ simulation time: N/A	2022	Freeware

Notes: [1] RANS = Reynolds-Averaged Navier–Stokes equations; RNG = Re-normalization Group; VOF = Volume of Fluid. [2] CICSAM = Compressive Interface Capturing Scheme for Arbitrary Meshes; MULES = Multidimensional Universal Limiter with Explicit Solution; PIMPLE = combination of PISO and SIMPLE; PISO = Pressure Implicit with Split Operators; SIMPLE = Semi-Implicit Method for Pressure-Linked Equations; SPH = Smoothed-Particle Hydrodynamics. [3] GPU = Graphics Processing Unit; MPI = Message Passing Interface. N/A = not available; * dam spillway or overtopping flow.

3. Results and Discussion

A total of 34 documents relating to the period from 2006 to the present were retrieved from the literature review. However, 39 entries appear in Table 2, as nine of the references examined present two different case studies, hence being repeated in two different table rows, and four references are mentioned together with other works that contain identical case studies.

Figure 3 summarises the main statistical information derived from the analysis of the papers reviewed. About a third of these (12) were published in the last three years (2020–2022), confirming a recent growing interest in 3D modelling of real-field dam-break flows (Figure 3a). In most case studies examined (43.6%), in-house research codes were adopted for the numerical analyses; commercial CFD software packages and open-source or freeware codes were used in 17.9% and 35.9% of cases, respectively (Figure 3b). The type of code was unspecified in only one case. Mesh-based methods appear in Table 2 more times (25) than particle-based ones (14) (Figure 3c). Among the former methods, the VOF-based finite volume ones are the most commonly used, whereas, among the latter, the SPH methods are prevalent. This state of the art was also observed by other researchers (e.g., [101]) who, in addition, showed how numerical results obtained from these two methods are in good agreement [102]. The Lattice Boltzmann method appears in Table 2 in only one case. This modern numerical technique still has limited application to dam-break problems [103,104]. Finite volume techniques are the most used in the reviewed papers for discretizing the governing equations in mesh-based models (Figure 3d). Indeed, the finite volume method is particularly suitable for solving conservation law equations because it exploits the integral formulation of the equations to capture their weak solutions [105]. Finite element methods appear fewer times in Table 2, since this numerical technique still constitutes a developing research area in CFD [106] and free surface flow modelling [107], despite its ability to treat complex geometries and reach high-order accuracy.

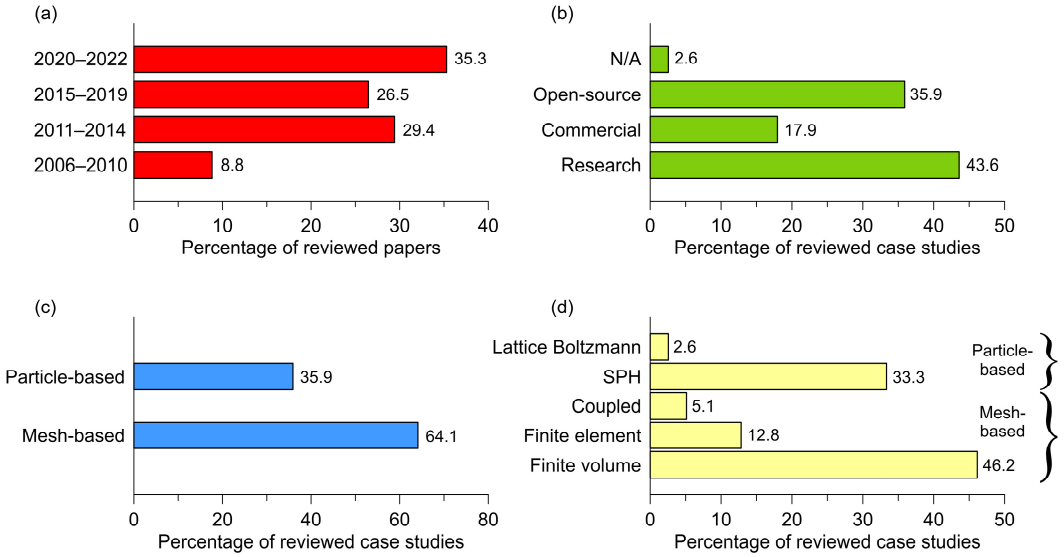

Figure 3. Statistical information from the database of the reviewed papers on 3D modelling of large-scale real-world dam-break floods: (**a**) year of publication; (**b**) status of the software; (**c**) model type; (**d**) numerical scheme.

The catastrophic scenario of the sudden and total dam collapse is mostly considered in the case studies reviewed, thus neglecting the breach development dynamics.

Three-dimensional models employed in dam-break modelling are also commonly used to simulate floods in rivers (e.g., [45,108]) or inundations in floodplains [19] or in urban areas (e.g., [36,109]).

3.1. Improvements in Simulation Accuracy

Three-dimensional hydrodynamic modelling improves the mathematical description of dam-break flows compared to routinely adopted 2D depth-averaged modelling, because 3D models overcome the intrinsic limitations of 2D ones. Therefore, 3D modelling is of wide applicability and general interest in dam-break problems. Indeed, 3D models calculate the pressure field and include the vertical fluid acceleration, thereby inherently taking into account the effects of flow curvature. Moreover, 3D models involve the vertical velocity component and describe the vertical variation of flow velocity. Conversely, 2D depth-averaged models introduce hypotheses on the vertical pressure distribution (assumed hydrostatic in SWE models) or the shape of the vertical velocity profile in non-hydrostatic flow models [23]. Finally, 3D models can include vertical turbulence and spiral flows [60] and can correctly simulate the impact of flows against obstacles or structures [109,110]. These enhanced modelling capabilities of 3D models can ensure more accurate flow predictions, especially around structures, at topographic singularities where sudden changes in the bottom surface occur, and in urban flooding simulations. Reproducing small-scale eddies, vertical turbulence, and residual circulation can be crucial for accurately predicting both near-field and far-field features of the flooding dynamics and the flow variables involved in flood hazard assessments.

The capabilities of 3D models were verified and validated in most of the articles reviewed, but the analysis of 3D flow effects is the focus of only a few of them (e.g., [70,71,82,87]). For example, Biscarini et al. [82] discussed the 3D effects induced on a dam-break flow by a sharp river bend. Even fewer are the articles that, based on a real-field case study, compare the results obtained through a 3D model with those obtained through a standard 2D depth-averaged shallow-water model, analysing the differences [37,50,80]. For example, Munoz and Constantinescu [37], studying the flood inundations induced by the hypothetical failure of two flood-protection dams in the United States, found that their 2D depth-averaged model underpredicted the wave propagation speed and the inundation extent compared with a 3D model. Most frequently, in the literature, the comparison of 3D and 2D model performance in predicting dam-break flow was made on the basis of schematic test cases characterised by a simple geometry (e.g., [27,111]).

In 3D models based on the RANS equations, the effect of turbulence is introduced through a closure turbulence model. The classic k-ε model is the most adopted in the references reviewed (entries [37,82,85,95] in Table 2). However, no systematic sensitivity analyses on the turbulence model type were performed for real-world dam-break case studies. The prediction capabilities of different turbulence models were typically compared again on the basis of dam-break test cases characterised by a simple and schematic geometry (e.g., [110,112–116]), exploiting laboratory experimental data.

Some references analysed in this review consider mudflows resulting from a tailings dam failure. In these studies, the tailings slurry is assumed as a homogeneous non-Newtonian viscoplastic fluid, and a suitable constitutive equation is added to the set of governing equations to characterise its rheological properties [88,91,92,99,100]. In some other studies among those reviewed, non-Newtonian rheological models are used to describe the behaviour of moving sediment layers in the path of the dam-break wave [90,98], thereby simulating the geomorphic effects produced by a dam-break flood on an erodible bed. An erosional dam break (with bed-load transport) on real-world topography was modelled by Amicarelli et al. [84] through an SPH model applied to a mixture of water and a non-cohesive granular material.

Recently, topographic data accuracy and spatial resolution have been significantly improved thanks to highly accurate terrain surveying techniques, such as scanning airborne laser altimetry (LIDAR), which can reach a horizontal resolution even below 1 m and a vertical accuracy of 10^{-1} m [19], and unmanned aerial vehicle (UAV) photogrammetry, which is very effective in terms of timeliness, repeatability, and high resolution [91]. Hence, highly accurate and high-resolution topographic digital models are widespread nowadays, even in urban areas [85], and allow for very accurate dam-break flow modelling.

On the other hand, despite the implicit greater descriptive capacity (and complexity) of 3D models, accuracy improvement in 3D numerical predictions compared with simpler, low-dimensional models may be illusory if topographic and input data are limited and inaccurate and reliable real-field validation data are scarce [19,117].

3.2. Model Validation and Calibration

Dam-break models are usually validated by comparing numerical results with experimental data [13]. To this end, real-field data of historical dam-break events or experimental data obtained from small-scale physical models with an irregular bottom can be very useful [14], especially if the numerical model will be used in practical engineering applications for dam-break inundation mapping and flood hazard assessment. Validation against real-field data can also help discriminate among potential competing models able to return plausible and realistic results.

Based on the articles reviewed, the most used real-field test case for validating 3D dam-break numerical models is the historical event of the 1959 Malpasset dam break (entries [75,82,83] in Table 2). An extensive database is available for this test case, including field data collected immediately after the event and data measured during a laboratory investigation in a reduced-scale physical model [118,119]. However, other historical dam-break events are well documented [14]; for some of these, the test case and the experimental data (from field surveys or consultation of historical documents) are available in digital format [120,121].

Another test case frequently used for validating 3D dam-break numerical models is the Toce River test case (entries [50,81,85,96] in Table 2), which concerns a dam-break-like flash flood induced by imposing an inflow discharge hydrograph in a 1:100 physical model of a 5 km long stretch of the Toce River valley in northern Italy [122]. An idealised urban district was inserted in this physical model to simulate the dam-break flooding of an urban area. Other experimental data from reduced-scale physical models are available in the literature [123,124] and could be considered for validating 3D dam-break models.

In complex 3D models, a large number of model parameters requiring calibration appear, mainly concerning numerical schemes and turbulence models. Accordingly, an optimization process involving many parameters should be performed, which might be challenging and computationally expensive due to the long runtime of each model execution. Therefore, calibration parameters are usually set based on expert judgement, according to the suggestions of software users' guides or following the choices made in similar numerical studies.

Uncertainty analysis is widely recognised as desirable, if not indispensable, in environmental system modelling to associate uncertainty estimates with model predictions [15]. In real-world applications of dam-break inundation modelling, the main uncertainty sources are topographic input data, model parameters (including the mesh resolution), and initial conditions defining the dam-break scenario (i.e., breach parameters and reservoir filling conditions). Modern remote sensing acquisition technologies (such as LIDAR) have drastically reduced the uncertainty in terrain description, and the availability of high-resolution topographic data makes it possible to include in the computational domain obstacles, structures, and topographic details that may significantly influence the inundation process [60]. The typical way to individually quantify the effects of model or scenario parameters on numerical predictions is to perform a sensitivity analysis based on a sampling approach (e.g., [125,126]). Monte Carlo methods are usually adopted to this end, considering a sample of the appropriate size to ensure convergence. However, exhaustive sensitivity analyses based on large sets of parameter values (and, consequently, many model runs) may be prohibitive using 3D hydrodynamic models. To overcome this limitation, Rizzo et al. [10] (who, however, used a 2D depth-averaged shallow-water model) proposed a probabilistic method based on a limited set of dam-break scenarios, each of which had a (conditional) probability associated with it. As regards the spatial resolution, Zhang et al. [87] performed a sensitivity analysis on the mesh size for a realistic dike-break flooding case, concluding

that the spatial resolution significantly impacts the accuracy of model results when the terrain is irregular, as in real-field applications.

3.3. Improvements in Computational Efficiency

The main reason for the limited use of 3D models in large-scale dam-break flood simulation over real-world topography is that they are time-consuming due to their high computational cost, which depends on various factors, such as the complexity of the numerical method adopted to solve the governing equations, the extent of the computational domain, the simulation (physical) time (usually set long enough to reconstruct the salient features of the flooding process), and the mesh type and resolution (in mesh-based models) or the particle size (in particle-based models). This problem—which is exacerbated in real-world applications—does not concern, as a rule, dam-break tests characterised by a schematic geometry (i.e., verification against analytical solutions or validation against laboratory data), because such simple tests do not require, in general, significant computational resources.

A viable option to overcome the limitation related to computational efficiency without resorting to approximate models [127] is to accelerate 3D model calculations via high-performance computing and GPU technology to reduce model running times [19]. In particular, parallel computing is a valid and widely used method to improve computational efficiency, possibly exploiting GPU computing power and processing capabilities.

Reducing the computational time of model executions also allows larger domains to be considered with high spatial resolution, extending the simulation of the flooding dynamics for a longer simulation time. Moreover, a large set of dam-break scenarios can be used in sensitivity analyses for assessing model uncertainty.

Table 2 shows that parallelization techniques based on Message Passing Interface (MPI; [39,72]) and the GPU implementation of the simulation model [77,86,91] were used in 3D modelling of real-field dam-break flows. The ratio of model run time to simulation time is highly variable, ranging from 10^2 to 10^4, depending on the number of processors and the total number of computational cells or particles. Yu et al. [92] analysed the gain in parallel speed-up as a function of the number of processors.

3.4. Improvements in Result Visualization

Geographic information systems (GISs; [72,73]) and 3D virtual geographic environment (VGE) systems have recently become attractive tools for the 3D dynamic visualization of model results, improving the communication of the dam-break flooding dynamics and the potential consequences (e.g., [128]). The availability of 3D numerical results facilitates the development of 3D virtual reality environments and visualizations, which, currently, are usually based on 2D hydraulic model data and results extrapolated into 3D (e.g., [129,130]).

4. Conclusions

Three-dimensional numerical modelling of dam-break flow has developed considerably in the last decade thanks to the significant increase in the available computing resources, which has made 3D modelling a viable alternative to routinely used 2D depth-averaged modelling in large-scale real-field applications, despite its higher computational cost. Even if 3D numerical models have only recently become a real and feasible option in large-scale dam-break modelling on real-world topography, we found in the literature a noticeable number of contributions concerning this fluid dynamic application, including standard dam-break water flows as well as geomorphic and tailings dam-break flows. Mesh-based models are mostly used for solving the governing hydrodynamic equations, which are the Navier–Stokes equations or the RANS equations coupled with a free-surface tracking technique (e.g., the VOF method) and a closure turbulence model. However, in recent years, particle-based models based on the SPH technique have become widespread in computational fluid dynamics and in the simulation of dam-break flows. Indeed, this method benefits from both being mesh-free and not requiring computationally expensive

free-surface tracking techniques. The application of the Lattice Boltzmann method to large-scale 3D dam-break flood modelling is a relatively new research field that deserves further exploration [96].

This paper systematically reviews the state-of-the-art 3D numerical modelling of large-scale dam-break floods on irregular real-world topography. The literature survey is mainly based on journal and conference papers published until July 2023, excluding the grey literature. We aimed to conduct an exhaustive and meticulous review based on comprehensive search parameters and inclusive keywords. Nevertheless, we may have missed studies published in journals of local diffusion or not specifically focused on 3D numerical modelling.

The references reviewed are organised into a table (Table 2) reporting extensive information on numerical models, case studies analysed, research focus, numerical results, and computational efficiency. Recent developments and key improvements in modelling and computational aspects, such as model accuracy and efficiency, are discussed. Regarding computational efficiency, code running on Graphics Processing Units and massive parallelization ensure a significant computational time reduction. This general improvement in computational efficiency allows for high spatial resolutions, even in large-scale applications. However, model calibration remains challenging due to the large number of parameters involved in 3D models, especially when coupled with a turbulence model. The 3D visualization of the numerical results can improve the quality of the communication of the dam-break flood hazard to managers and stakeholders, thus contributing to the mitigation of dam-break flood consequences.

Compared to the less computationally demanding 2D depth-averaged models, the 3D ones allow for a more detailed and accurate prediction of the flooding dynamics, inherently including the fluid vertical acceleration and 3D effects due to the flow curvature induced by the irregular topography. Freeware and commercial CFD software (relatively user-friendly) are available nowadays for dam-break flow analysis, even concerning large-scale problems on real-world topography.

Future research may concern coupled 2D–3D models as a valid compromise between simulation accuracy and computational efficiency. This modelling option is currently already introduced in some CFD software (e.g., [131]) in order to simulate large-scale flows in which the shallow water assumptions are approximately valid with a 2D depth-averaged model, and near-field flows and localised flow features (near structures, obstacles, or significant topographic irregularities) with a 3D model. For instance, hybrid 2D–3D models could be used to simulate dam-break flooding generated by a partial dam failure, with the breach involving only the upper part of the dam. In this case, the weir-type outflow could be modelled by the 3D model and the wave propagation in the downstream area by the 2D depth-averaged model. The portions of the computational domain in which to apply the two different models can be previously identified and efficiently linked.

This review can guide researchers, modellers, and practitioners to compare existing 3D dam-break numerical models, choose the most suitable model for the application of interest, and select state-of-the-art numerical approaches. This review can also support modellers and researchers, providing a basis for future research in 3D simulation models and computational techniques for dam-break flow modelling, with special attention to large-scale real-field applications.

Author Contributions: A.M. and M.T. contributed equally to the conceptualization and implementation of the research, the revision of the existing literature, the analysis of results, and the writing of the manuscript. All authors have read and agreed to the published version of the manuscript.

Funding: A.M. was supported by the Italian Ministry of University and Research through the PRIN 2017 Project RELAID (REnaissance of LArge Italian Dams), project number 2017T4JC5K.

Data Availability Statement: No new data were created or analysed in this study. Data sharing is not applicable to this article.

Conflicts of Interest: The authors declare no conflict of interest.

References

1. Costa, J.E. *Floods from Dam Failures*; Open-File Report 85-560; US Geological Survey: Denver, CO, USA, 1985. Available online: https://pubs.usgs.gov/of/1985/0560/report.pdf (accessed on 21 July 2023).
2. Charles, J.A.; Tedd, P.; Warren, A. *Lessons from Historical Dam Incidents*; Project SC080046/R1; Environment Agency: Bristol, UK, 2011. Available online: https://assets.publishing.service.gov.uk/media/603369e7e90e07660cc43890/_Lessons_from_Historical_Dam_Incidents_Technical_Report.pdf (accessed on 21 July 2023).
3. Zhang, L.; Peng, M.; Chang, D.; Xu, Y. *Dam Failure Mechanisms and Risk Assessment*; Wiley: Singapore, 2016.
4. Graham, W.J. *A Procedure for Estimating Loss of Life Caused by Dam Failure*; DSO-99-06; US Department of Interior, Bureau of Reclamation, Dam Safety Office: Denver, CO, USA, 1999. Available online: https://www.usbr.gov/ssle/damsafety/TechDev/DSOTechDev/DSO-99-06.pdf (accessed on 21 July 2023).
5. ASDSO (Association of State Dam Safety Officials). Lesson Learned from Dam Incidents and Failures—Case Studies. Available online: https://damfailures.org/case-study/ (accessed on 21 July 2023).
6. International Water Power and Dam Construction. Learning Historical Dam Safety Lessons. Available online: https://www.waterpowermagazine.com/features/featurelearning-historical-dam-safety-lessons-4958949/ (accessed on 21 July 2023).
7. FEMA. *Federal Guidelines for Inundation Mapping of Flood Risks Associated with Dam Incidents and Failures*; FEMA P-946; Federal Emergency Management Agency, US Department of Homeland Security: Washington, DC, USA, 2013. Available online: https://www.fema.gov/sites/default/files/2020-08/fema_dam-safety_inundation-mapping-flood-risks.pdf (accessed on 25 May 2023).
8. CDSO. *Guidelines for Mapping Flood Risk Associated with Dams*; CDSO_GUD_DS_05_v1.0; Central Dam Safety Organization, Central Water Commission, Dam Safety Rehabilitation Directorate: New Delhi, India, 2018. Available online: https://damsafety.cwc.gov.in/ecm-includes/PDFs/Guidelines_for_Mapping_Flood_Risks_Associated_with_Dams.pdf (accessed on 25 May 2023).
9. Morris, M.W. *CADAM Concerted Action on Dam Break Modeling*; Final Report SR 571; HR Wallingford: Oxford, UK, 2000; Available online: https://eprints.hrwallingford.com/447/1/CADAM.pdf (accessed on 25 May 2023).
10. Rizzo, C.; Maranzoni, A.; D'Oria, M. Probabilistic Mapping and Sensitivity Assessment of Dam-Break Flood Hazard. *Hydrol. Sci. J.* **2023**, *68*, 700–718. [CrossRef]
11. Maranzoni, A.; D'Oria, M.; Rizzo, C. Quantitative Flood Hazard Assessment Methods: A Review. *J. Flood Risk Manag.* **2023**, *16*, e12855. [CrossRef]
12. Ferrari, A.; Vacondio, R.; Mignosa, P. High-Resolution 2D Shallow Water Modelling of Dam Failure Floods for Emergency Action Plans. *J. Hydrol.* **2023**, *618*, 129192. [CrossRef]
13. Aureli, F.; Maranzoni, A.; Petaccia, G.; Soares-Frazão, S. Review of Experimental Investigations of Dam-Break Flows over Fixed Bottom. *Water* **2023**, *15*, 1229. [CrossRef]
14. Aureli, F.; Maranzoni, A.; Petaccia, G. Review of Historical Dam-Break Events and Laboratory Tests on Real Topography for the Validation of Numerical Models. *Water* **2021**, *13*, 1968. [CrossRef]
15. Teng, J.; Jakeman, A.J.; Vaze, J.; Croke, B.F.W.; Dutta, D.; Kim, S. Flood Inundation Modelling: A Review of Methods, Recent Advances and Uncertainty Analysis. *Environ. Model. Softw.* **2017**, *90*, 201–216. [CrossRef]
16. De Marchi, G. Sull'Onda di Piena che Seguirebbe al Crollo della Diga di Cancano [On the Dam-Break Wave Resulting from the Collapse of the Cancano Dam]. *L'Energia Elettr.* **1945**, *22*, 157–169. (In Italian)
17. Antunes do Carmo, J.S. Physical Modelling vs. Numerical Modelling: Complementarity and Learning. *Preprints* **2020**, 2020070753. Available online: https://www.preprints.org/manuscript/202007.0753/v2/download (accessed on 21 July 2023).
18. Mudashiru, R.B.; Sabtu, N.; Abustan, I.; Balogun, W. Flood Hazard Mapping Methods: A Review. *J. Hydrol.* **2021**, *603*, 126846. [CrossRef]
19. Bates, P.D. Flood Inundation Prediction. *Annu. Rev. Fluid Mech.* **2022**, *54*, 287–315. [CrossRef]
20. Toro, E.F.; Garcia-Navarro, P. Godunov-Type Methods for Free-Surface Shallow Flows: A Review. *J. Hydraul. Res.* **2007**, *45*, 736–751. [CrossRef]
21. Castro-Orgaz, O.; Hager, W.H. *Shallow Water Hydraulics*; Springer: Cham, Switzerland, 2019.
22. Toro, E.F. *Shock-Capturing Methods for Free-Surface Shallow Flows*; John Wiley & Sons: Chichester, UK, 2001.
23. Castro-Orgaz, O.; Hager, W.H. *Non-Hydrostatic Free Surface Flows*; Springer: Cham, Switzerland, 2017.
24. Maranzoni, A.; Tomirotti, M. New Formulation of the Two-Dimensional Steep-Slope Shallow Water Equations. Part I: Theory and Analysis. *Adv. Water Resour.* **2022**, *166*, 104255. [CrossRef]
25. Maranzoni, A.; Tomirotti, M. New Formulation of the Two-Dimensional Steep-Slope Shallow Water Equations. Part II: Numerical Modeling, Validation, and Application. *Adv. Water Resour.* **2023**, *177*, 104403. [CrossRef]
26. Stansby, P.K.; Chegini, A.; Barnes, T.C.D. The Initial Stages of Dam-Break Flow. *J. Fluid Mech.* **1998**, *374*, 407–424. [CrossRef]
27. Ozmen-Cagatay, H.; Kocaman, S. Dam-Break Flows During Initial Stage Using SWE and RANS Approaches. *J. Hydraul. Res.* **2010**, *48*, 603–611. [CrossRef]
28. Soares-Frazão, S.; Zech, Y. Dam Break in Channels with 90° Bend. *J. Hydraul. Eng.* **2002**, *128*, 956–968. [CrossRef]
29. Kocaman, S.; Ozmen-Cagatay, H. The Effect of Lateral Channel Contraction on Dam Break Flows: Laboratory Experiment. *J. Hydrol.* **2012**, *432–433*, 145–153. [CrossRef]
30. Khoshkonesh, A.; Nsom, B.; Bahmanpouri, F.; Dehrashid, F.A.; Adeli, A. Numerical Study of the Dynamics and Structure of a Partial Dam-Break Flow Using the VOF Method. *Water Resour. Manage.* **2021**, *35*, 1513–1528. [CrossRef]

31. Soares-Frazão, S. Experiments of Dam-Break Wave Over a Triangular Bottom Sill. *J. Hydraul. Res.* **2007**, *45* (Suppl. S1), 19–26. [CrossRef]
32. Ozmen-Cagatay, H.; Kocaman, S.; Guzel, H. Investigation of Dam-Break Flood Waves in a Dry Channel with a Hump. *J. Hydro-Environ. Res.* **2014**, *8*, 304–315. [CrossRef]
33. Soares-Frazão, S.; Zech, Y. Experimental Study of Dam-Break Flow against an Isolated Obstacle. *J. Hydraul. Res.* **2007**, *45* (Suppl. S1), 27–36. [CrossRef]
34. Aureli, F.; Dazzi, S.; Maranzoni, A.; Mignosa, P.; Vacondio, R. Experimental and Numerical Evaluation of the Force Due to the Impact of a Dam-Break Wave on a Structure. *Adv. Water Resour.* **2015**, *76*, 29–42. [CrossRef]
35. Khoshkonesh, A.; Daliri, M.; Riaz, K.; Dehrashid, F.A.; Bahmanpouri, F.; Di Francesco, S. Dam-Break Flow Dynamics over a Stepped Channel with Vegetation. *J. Hydrol.* **2022**, *613*, 128395. [CrossRef]
36. Zhang, T.; Feng, P.; Maksimović, Č.; Bates, P.D. Application of a Three-Dimensional Unstructured-Mesh Finite-Element Flooding Model and Comparison with Two-Dimensional Approaches. *Water Resour. Manage.* **2016**, *30*, 823–841. [CrossRef]
37. Munoz, D.H.; Constantinescu, G. 3-D Dam Break Flow Simulations in Simplified and Complex Domains. *Adv. Water Resour.* **2020**, *137*, 103510. [CrossRef]
38. Fernandez-Feria, R. Dam-Break Flow for Arbitrary Slopes of the Bottom. *J. Eng. Math.* **2006**, *54*, 319–331. [CrossRef]
39. Castro-Orgaz, O.; Cantero-Chinchilla, F.N. Non-Linear Shallow Water Flow Modelling over Topography with Depth-Averaged Potential Equations. *Environ. Fluid Mech.* **2020**, *20*, 261–291. [CrossRef]
40. Lu, X.; Dong, B.; Zhang, X. A Two-Dimensional Depth-Integrated Non-Hydrostatic Numerical Model for Nearshore Wave Propagation. *Ocean Model.* **2015**, *96*, 187–202. [CrossRef]
41. Cantero-Chinchilla, F.N.; Bergillos, R.J.; Gamero, P.; Castro-Orgaz, O.; Cea, L.; Hager, W.H. Vertically Averaged and Moment Equations for Dam-Break Wave Modeling: Shallow Water Hypotheses. *Water* **2020**, *12*, 3232. [CrossRef]
42. Denlinger, R.P.; Iverson, R.M. Granular Avalanches Across Irregular Three-Dimensional Terrain: 1. Theory and Computation. *J. Geophys. Res. Earth Surf.* **2004**, *109*, F01014. [CrossRef]
43. Denlinger, R.P.; O'Connell, D.R. Computing Nonhydrostatic Shallow-Water Flow over Steep Terrain. *J. Hydraul. Eng.* **2008**, *134*, 1590–1602. [CrossRef]
44. Biscarini, C.; Di Francesco, S.; Manciola, P. CFD Modelling Approach for Dam Break Flow Studies. *Hydrol. Earth Syst. Sci.* **2010**, *14*, 705–718. [CrossRef]
45. Lane, S.N.; Bradbrook, K.F.; Richards, K.S.; Biron, P.A.; Roy, A.G. The Application of Computational Fluid Dynamics to Natural River Channels: Three-Dimensional Versus Two-Dimensional Approaches. *Geomorphology* **1999**, *29*, 1–20. [CrossRef]
46. Versteeg, H.K.; Malalasekera, W. *An Introduction to Computational Fluid Dynamics. The Finite Volume Method*; Longman Scientific & Technical: Harlow, UK, 1995.
47. Hirt, C.W.; Nichols, B.D. Volume of Fluid (VOF) Methods for the Dynamics of Free Boundaries. *J. Comput. Phys.* **1981**, *39*, 201–225. [CrossRef]
48. Osher, S.; Fedkiw, R.P. Level Set Methods: An Overview and Some Recent Results. *J. Comput. Phys.* **2001**, *169*, 463–502. [CrossRef]
49. Sussman, M.; Puckett, E.G. A Coupled Level Set and Volume-of-Fluid Method for Computing 3D and Axisymmetric Incompressible Two-Phase Flows. *J. Comput. Phys.* **2000**, *162*, 301–337. [CrossRef]
50. Marsooli, R.; Wu, W. 3-D Finite-Volume Model of Dam-Break Flow over Uneven Beds Based on VOF Method. *Adv. Water. Resour.* **2014**, *70*, 104–117. [CrossRef]
51. Monaghan, J.J. Simulating Free Surface Flows with SPH. *J. Comput. Phys.* **1994**, *110*, 399–406. [CrossRef]
52. Xu, X. An Improved SPH Approach for Simulating 3D Dam-Break Flows with Breaking Waves. *Comput. Methods Appl. Mech. Eng.* **2016**, *311*, 723–742. [CrossRef]
53. Xu, X.; Jiang, Y.-L.; Yu, P. SPH Simulations of 3D Dam-Break Flow Against Various Forms of the Obstacle: Toward an Optimal Design. *Ocean Eng.* **2021**, *229*, 108978. [CrossRef]
54. Cleary, P.W.; Prakash, M. Discrete-Element Modelling: Methods and Applications in the Environmental Sciences. *Phil. Trans. R. Soc. Lond. A* **2004**, *362*, 2003–2030. [CrossRef] [PubMed]
55. Wu, J.; Bao, K.; Zhang, H. Research Progress on Dam-Break Floods. In Proceedings of the 2nd IEEE International Conference on Emergency Management and Management Sciences, Beijing, China, 8–10 August 2011; pp. 334–338. [CrossRef]
56. Ferrari, A.; Fraccarollo, L.; Dumbser, M.; Toro, E.F.; Armanini, A. Three-Dimensional Flow Evolution after a Dam Break. *J. Fluid Mech.* **2010**, *663*, 456–477. [CrossRef]
57. Xie, Z.; Stoesser, T.; Xia, J. Simulation of Three-Dimensional Free-Surface Dam-Break Flows over a Cuboid, Cylinder, and Sphere. *J. Hydraul. Eng.* **2021**, *147*, 6021009. [CrossRef]
58. Issakhov, A.; Imanberdiyeva, M. Numerical Simulation of the Movement of Water Surface of Dam Break Flow by VOF Methods for Various Obstacles. *Int. J. Heat Mass Transf.* **2019**, *136*, 1030–1051. [CrossRef]
59. Issakhov, A.; Borsikbayeva, A. The Impact of a Multilevel Protection Column on the Propagation of a Water Wave and Pressure Distribution During a Dam Break: Numerical Simulation. *J. Hydrol.* **2021**, *598*, 126212. [CrossRef]
60. Luo, P.; Luo, M.; Li, F.; Qi, X.; Huo, A.; Wang, Z.; He, B.; Takara, K.; Nover, D.; Wang, Y. Urban Flood Numerical Simulation: Research, Methods and Future Perspectives. *Environ. Model. Softw.* **2022**, *156*, 105478. [CrossRef]
61. Mignot, E.; Dewals, B. Hydraulic Modelling of Inland Urban Flooding: Recent Advances. *J. Hydrol.* **2022**, *609*, 127763. [CrossRef]

62. Kumar, V.; Sharma, K.V.; Caloiero, T.; Mehta, D.J.; Singh, K. Comprehensive Overview of Flood Modeling Approaches: A Review of Recent Advances. *Hydrology* **2023**, *10*, 141. [CrossRef]
63. Avila-Aceves, E.; Plata-Rocha, W.; Monjandin-Armenta, S.A.; Rangel-Peraza, J.G. Geospatial Modelling of Floods: A Literature Review. *Stoch. Environ. Res. Risk Assess.* **2023**. [CrossRef]
64. TELEMAC-3D—3D Hydrodynamics. Available online: http://www.opentelemac.org/index.php/presentation?id=18 (accessed on 27 March 2023).
65. FLOW-3D. Available online: https://www.flow3d.com/products/flow-3d/ (accessed on 27 March 2023).
66. About OpenFOAM. Available online: https://www.openfoam.com/ (accessed on 27 March 2023).
67. DualSPHysics: From Fluid Dynamics to Multiphysics Problems. Available online: https://dual.sphysics.org/ (accessed on 5 April 2023).
68. Amicarelli, A.; Manenti, S.; Albano, R.; Agate, G.; Paggi, M.; Longoni, L.; Mirauda, D.; Ziane, L.; Viccione, G.; Todeschini, S.; et al. SPHERA v. 9.0.0: A Computational Fluid Dynamics Research Code, Based on the Smoothed Particle Hydrodynamics Mesh-Less Method. *Comput. Phys. Commun.* **2020**, *250*, 107157. [CrossRef]
69. Roubtsova, V.; Kahawita, R. The SPH Technique Applied to Free Surface Flows. *Comput. Fluids* **2006**, *35*, 1359–1371. [CrossRef]
70. Cleary, P.W.; Prakash, M.; Rothauge, K. Combining Digital Terrain and Surface Textures with Large-Scale Particle-Based Computational Models to Predict Dam Collapse and Landslide Events. *Int. J. Image Data Fusion* **2010**, *1*, 337–357. [CrossRef]
71. Prakash, M.; Rothauge, K.; Cleary, P.W. Modelling the Impact of Dam Failure Scenarios on Flood Inundation Using SPH. *Appl. Math. Model.* **2014**, *38*, 5515–5534. [CrossRef]
72. Ye, F.; Wang, H.; Ouyang, S.; Tang, X.; Li, Z.; Prakash, M. Spatio-Temporal Analysis and Visualization Using SPH for Dam-Break and Flood Disasters in a GIS Environment. In Proceedings of the 2012 International Symposium on Geomatics for Integrated Water Resource Management, Lanzhou, China, 19–21 October 2012. [CrossRef]
73. Cleary, P.W.; Prakash, M.; Mead, S.; Tang, X.; Wang, H.; Ouyang, S. Dynamic Simulation of Dam-Break Scenarios for Risk Analysis and Disaster Management. *Int. J. Image Data Fusion* **2012**, *3*, 333–363. [CrossRef]
74. Lee, E.-S.; Violeau, D.; Issa, R.; Ploix, S. Application of Weakly Compressible and Truly Incompressible SPH to 3-D Water Collapse in Waterworks. *J. Hydraul. Res.* **2010**, *48* (Suppl. S1), 50–60. [CrossRef]
75. Caboussat, A.; Boyaval, S.; Masserey, A. On the Modeling and Simulation of Non-Hydrostatic Dam Break Flows. *Comput. Visual. Sci.* **2011**, *14*, 401–417. [CrossRef]
76. Vassilevski, Y.V.; Nikitin, K.D.; Olshanskii, M.A.; Terekhov, K.M. CFD Technology for 3D Simulation of Large-Scale Hydrodynamic Events and Disasters. *Russ. J. Numer. Anal. Math. Model.* **2012**, *27*, 399–412. [CrossRef]
77. Vacondio, R.; Mignosa, P.; Pagani, S. 3D SPH Numerical Simulation of the Wave Generated by the Vajont Rockslide. *Adv. Water Res.* **2013**, *59*, 146–156. [CrossRef]
78. Zhainakov, A.Z.; Kurbanaliev, A.Y. Verification of the Open Package OpenFOAM on Dam Break Problems. *Thermophys. Aeromech.* **2013**, *20*, 451–461. [CrossRef]
79. Jainakov, A.; Kurbanaliev, A.; Oskonbaev, M. Large-Scale Modeling of Dam Break Induced Flows. In *Dam Engineering*; Tosun, H., Ed.; IntechOpen: London, UK, 2019; pp. 59–72. [CrossRef]
80. Džebo, E.; Žagar, D.; Krzyk, M.; Četina, M.; Petkovšek, G. Different Ways of Defining Wall Shear in Smoothed Particle Hydrodynamics Simulations of a Dam-Break Wave. *J. Hydraul. Res.* **2014**, *52*, 453–464. [CrossRef]
81. Zhou, Z.; Wang, X.; Sun, R.; Ao, X.; Sun, X.; Song, M. Study of the Comprehensive Risk Analysis of Dam-Break Flooding Based on the Numerical Simulation of Flood Routing. Part II: Model Application and Results. *Nat. Hazards* **2014**, *72*, 675–700. [CrossRef]
82. Biscarini, C.; Di Francesco, S.; Ridolfi, E.; Manciola, P. On the Simulation of Floods in a Narrow Bending Valley: The Malpasset Dam Break Case Study. *Water* **2016**, *8*, 545. [CrossRef]
83. TELEMAC Modelling System. *3D Hydrodynamics, TELEMAC-3D Software*; Version 7.0, Validation Document; EDF R&D: Paris, France, 2016; Available online: http://www.opentelemac.org/index.php/component/jdownloads/summary/44-v7p0/1302-telemac3d-validation-v7p0?Itemid=54 (accessed on 30 March 2023).
84. Amicarelli, A.; Kocak, B.; Sibilla, S.; Grabe, J. A 3D Smoothed Particle Hydrodynamics Model for Erosional Dam-Break Floods. *Int. J. Comput. Fluid Dyn.* **2017**, *31*, 413–434. [CrossRef]
85. Wang, X.; Chen, W.; Zhou, Z.; Zhu, Y.; Wang, C.; Liu, Z. Three-Dimensional Flood Routing of a Dam Break Based on a High-Precision Digital Model of a Dense Urban Area. *Nat. Hazards* **2017**, *86*, 1147–1174. [CrossRef]
86. Wang, K.; Yang, P.; Hudson-Edwards, K.A.; Lyu, W.; Yang, C.; Jing, X. Integration of DSM and SPH to Model Tailings Dam Failure Run-Out Slurry Routing Across 3D Real Terrain. *Water* **2018**, *10*, 1087. [CrossRef]
87. Zhang, T.; Peng, L.; Feng, P. Evaluation of a 3D Unstructured-Mesh Finite Element Model for Dam-Break Floods. *Comput. Fluids* **2018**, *160*, 64–77. [CrossRef]
88. Chen, H.-X.; Li, J.; Feng, S.-J.; Gao, H.-Y.; Zhang, D.-M. Simulation of Interactions Between Debris Flow and Check Dams on Three-Dimensional Terrain. *Eng. Geol.* **2019**, *251*, 48–62. [CrossRef]
89. Kurbanaliev, A.I.; Maksutov, A.R.; Obodoeva, G.S.; Oichueva, B.R. Using OpenFOAM Multiphase Solver InterFoam for Large Scale Modeling. In *Proceedings of the 27th World Congress on Engineering and Computer Science, San Francisco, CA, USA, 22–24 October 2019*; International Association of Engineers: Hong Kong, China; pp. 366–370. Available online: https://www.iaeng.org/publication/WCECS2019/WCECS2019_pp366-370.pdf (accessed on 25 August 2023).

90. Issakhov, A.; Zhandaulet, Y. Numerical Study of Dam Break Waves on Movable Beds for Complex Terrain by Volume of Fluid Method. *Water Resour. Manage.* **2020**, *34*, 463–480. [CrossRef]
91. Wang, K.; Yang, P.; Yu, G.; Yang, C.; Zhu, L. 3D Numerical Modelling of Tailings Dam Breach Run Out Flow over Complex Terrain: A Multidisciplinary Procedure. *Water* **2020**, *12*, 2538. [CrossRef]
92. Yu, D.; Tang, L.; Chen, C. Three-Dimensional Numerical Simulation of Mud Flow from a Tailing Dam Failure Across Complex Terrain. *Nat. Hazards Earth Syst. Sci.* **2020**, *20*, 727–741. [CrossRef]
93. Zhuang, Y.; Yin, Y.; Xing, A.; Jin, K. Combined Numerical Investigation of the Yigong Rock Slide-Debris Avalanche and Subsequent Dam-Break Flood Propagation in Tibet, China. *Landslides* **2020**, *17*, 2217–2229. [CrossRef]
94. Amicarelli, A.; Manenti, S.; Paggi, M. SPH Modelling of Dam-break Floods, with Damage Assessment to Electrical Substations. *Int. J. Comput. Fluid Dyn.* **2021**, *35*, 3–21. [CrossRef]
95. Karam, W.; Khan, F.A.; Alam, M.; Ali, S. Simulation of Dam-Break Flood Wave and Inundation Mapping: A Case Study of Attabad Lake. *Int. J.* **2021**, *9*, 703–714. [CrossRef]
96. Miliani, S.; Montessori, A.; La Rocca, M.; Prestininzi, P. Dam-Break Modeling: LBM as the Way Towards Fully 3D, Large-Scale Applications. *J. Hydraul. Eng.* **2021**, *147*, 4021017. [CrossRef]
97. Ai, C.; Ma, Y.; Ding, W.; Xie, Z.; Dong, G. Three-Dimensional Non-Hydrostatic Model for Dam-Break Flows. *Phys. Fluids* **2022**, *34*, 22105. [CrossRef]
98. Issakhov, A.; Borsikbayeva, A.; Abylkassymova, A.; Issakhov, A.; Khikmetov, A. Numerical Modeling of the Dam-Break Flood over Natural Rivers on Movable Beds. *Int. J. Nonlinear Sci. Numer. Simul.* **2022**. [CrossRef]
99. Yang, Y.; Zhou, X.; Chen, X.; Xie, C. Numerical Simulation of Tailings Flow from Dam Failure over Complex Terrain. *Materials* **2022**, *15*, 2288. [CrossRef] [PubMed]
100. Zhuang, Y.; Jin, K.; Cheng, Q.; Xing, A.; Luo, H. Experimental and Numerical Investigations of a Catastrophic Tailings Dam Break in Daye, Hubei, China. *Bull. Eng. Geol. Environ.* **2022**, *81*, 9. [CrossRef]
101. Jiang, H.; Zhao, B.; Dapeng, Z.; Zhu, K. Numerical Simulation of Two-Dimensional Dam Failure and Free-Side Deformation Flow Studies. *Water* **2023**, *15*, 1515. [CrossRef]
102. Oertel, M.; Bung, D.B. Comparison of 2D Dam-Break Waves with VOF and SPH Method. In *Proceedings of the 35th IAHR World Congress, Chengdu, China, 8–13 September 2013*; Tsinghua University Press: Beijing, China. Available online: https://www.iahr.org/library/infor?pid=14676 (accessed on 24 August 2023).
103. Purbasari, R.J.; Suryanto, A.; Anam, S. Numerical Simulations of Dam-Break Flows by Lattice Boltzmann Method. *AIP Conf. Proc.* **2021**, *2021*, 60027. [CrossRef]
104. Maquignon, N.; Smaoui, H.; Sergent, P.; Bader, B. A Simplified and Stable Lattice Boltzmann Shallow Water Model. *J. Phys. Conf. Ser.* **2022**, *2202*, 12055. [CrossRef]
105. LeVeque, R.J. *Finite Volume Methods for Hyperbolic Problems*; Cambridge University Press: Cambridge, UK, 2002.
106. Dick, E. Introduction to Finite Element Methods in Computational Fluid Dynamics. In *Computational Fluid Dynamics*, 3rd ed.; Wendt, J.F., Ed.; Springer: Berlin, Germany, 2009; pp. 235–274.
107. Hervouet, J.-M. *Hydrodynamics of Free Surface Flows: Modelling with the Finite Element Method*; Wiley: Chichester, UK, 2007.
108. Munoz, D.H.; Constantinescu, G. A Fully 3-D Numerical Model to Predict Flood Wave Propagation and Assess Efficiency of Flood Protection Measures. *Adv. Water Resour.* **2018**, *122*, 148–165. [CrossRef]
109. Rong, Y.; Zhang, T.; Zheng, Y.; Hu, C.; Peng, L.; Feng, P. Three-Dimensional Urban Flood Inundation Simulation Based on Digital Aerial Photogrammetry. *J. Hydrol.* **2020**, *584*, 124308. [CrossRef]
110. Peng, L.; Zhang, T.; Li, J.; Feng, P. Three-Dimensional Numerical Study of Dam-Break Flood Impacting Problem with VOF Method and Different Turbulence Closures. *Water Resour. Manage.* **2023**, *37*, 3875–3895. [CrossRef]
111. Pu, J.H.; Shao, S.; Huang, Y.; Hussain, K. Evaluations of SWEs and SPH Numerical Modelling Techniques for Dam Break Flows. *Eng. Appl. Comput. Fluid Mech.* **2013**, *7*, 544–563. [CrossRef]
112. Issakhov, A.; Zhandaulet, Y.; Nogaeva, A. Numerical Simulation of Dam Break Flow for Various Forms of the Obstacle by VOF Method. *Int. J. Multiph. Flow* **2018**, *109*, 191–206. [CrossRef]
113. Park, I.-R.; Kim, K.-S.; Kim, J.; Van, S.-H. Numerical Investigation of the Effects of Turbulence Intensity on Dam-Break Flows. *Ocean Eng.* **2012**, *42*, 176–187. [CrossRef]
114. Larocque, L.A.; Imran, J.; Chaudhry, M.H. 3D Numerical Simulation of Partial Breach Dam-Break Flow Using the LES and k–ϵ Turbulence Models. *J. Hydraul. Res.* **2013**, *51*, 145–157. [CrossRef]
115. Yang, S.; Yang, W.; Qin, S.; Li, Q. Comparative Study on Calculation Methods of Dam-Break Wave. *J. Hydraul. Res.* **2019**, *57*, 702–714. [CrossRef]
116. Simsek, O.; Islek, H. 2D and 3D Numerical Simulations of Dam-Break Flow Problem with RANS, DES, and LES. *Ocean Eng.* **2023**, *276*, 114298. [CrossRef]
117. Neal, J.; Villanueva, I.; Wright, N.; Willis, T.; Fewtrell, T.; Bates, P. How Much Physical Complexity is Needed to Model Flood Inundation? *Hydrol. Process.* **2012**, *26*, 2264–2282. [CrossRef]
118. Goutal, N. The Malpasset Dam Failure. An Overview and Test Case Definition. In Proceedings of the 4th CADAM Meeting, Zaragoza, Spain, 18–19 November 1999.
119. Hervouet, J.-M.; Petitjean, A. Malpasset Dam-Break Revisited with Two-Dimensional Computations. *J. Hydraul. Res.* **1999**, *37*, 777–788. [CrossRef]

120. Alcrudo, F.; Mulet, J. Description of the Tous Dam Break Case Study (Spain). *J. Hydraul. Res.* **2007**, *45* (Suppl. S1), 45–57. [CrossRef]
121. Pilotti, M.; Maranzoni, A.; Tomirotti, M.; Valerio, G. 1923 Gleno Dam Break: Case Study and Numerical Modeling. *J. Hydraul. Eng.* **2011**, *137*, 480–492. [CrossRef]
122. Testa, G.; Zuccalà, D.; Alcrudo, F.; Mulet, J.; Soares-Frazão, S. Flash Flood Flow Experiment in a Simplified Urban District. *J. Hydraul. Res.* **2007**, *45* (Suppl. S1), 37–44. [CrossRef]
123. Pilotti, M.; Milanesi, L.; Bacchi, V.; Tomirotti, M.; Maranzoni, A. Dam-Break Wave Propagation in Alpine Valley with HEC-RAS 2D: Experimental Cancano Test Case. *J. Hydraul. Eng.* **2020**, *146*, 5020003. [CrossRef]
124. Güney, M.S.; Tayfur, G.; Bombar, G.; Elci, S. Distorted Physical Model to Study Sudden Partial Dam Break Flows in an Urban Area. *J. Hydraul. Eng.* **2014**, *140*, 5014006. [CrossRef]
125. Norton, J. An Introduction to Sensitivity Assessment of Simulation Models. *Environ. Model. Softw.* **2015**, *69*, 166–174. [CrossRef]
126. Pianosi, F.; Beven, K.; Freer, J.; Hall, J.W.; Rougier, J.; Stephenson, D.B.; Wagener, T. Sensitivity Analysis of Environmental Models: A Systematic Review with Practical Workflow. *Environ. Model. Softw.* **2016**, *79*, 214–232. [CrossRef]
127. Castro-Orgaz, O.; Hager, W.H.; Katopodes, N.D. Variational Models for Nonhydrostatic Free-Surface Flow: A Unified Outlook to Maritime and Open-Channel Hydraulics Developments. *J. Hydraul. Eng.* **2023**, *149*, 4023014. [CrossRef]
128. Yu, D.; Tang, L.; Ye, F.; Chen, C. A Virtual Geographic Environment for Dynamic Simulation and Analysis of Tailings Dam Failure. *Int. J. Digit. Earth* **2021**, *14*, 1194–1212. [CrossRef]
129. Macchione, F.; Costabile, P.; Costanzo, C.; De Santis, R. Moving to 3-D Flood Hazard Maps for Enhancing Risk Communication. *Environ. Model. Softw.* **2019**, *111*, 510–522. [CrossRef]
130. Spero, H.R.; Vazquez-Lopez, I.; Miller, K.; Joshaghani, R.; Cutchin, S.; Enterkine, J. Drones, Virtual Reality, and Modeling: Communicating Catastrophic Dam Failure. *Int. J. Digit. Earth* **2022**, *15*, 585–605. [CrossRef]
131. FLOW-3D Modeling Capabilities. Hybrid Shallow Water/3D Flow. Available online: https://www.flow3d.com/modeling-capabilities/hybrid-shallow-water-3d-flow/ (accessed on 27 April 2023).